Journal of
MATERIALS RESEARCH

Estimation of hardness by nanoindentation of rough surfaces

M. S. Bobji and S. K. Biswas
Department of Mechanical Engineering, Indian Institute of Science, Bangalore, 560 012, India

(Received 22 July 1997; accepted 10 February 1998)

The roughness of a surface influences the surface mechanical properties, estimated using nanoindentation data. Assuming a relation between the penetration depth normalized with respect to a roughness scale parameter, and the effective radius encountered by the indenter, a first order model of roughness dependency of hardness is proposed. The practical usefulness of this model is verified by the numerical simulation of nanoindentation on a fractal surface. As the roughness of a surface is increased, the hardness measured at depths comparable with the roughness scale deviates increasingly from the actual hardness. Given the constants related to indenter geometry, the present work provides a rationale and a method for deconvoluting the effect of roughness in arriving at real hardness characteristics of the near surface region of a material.

I. INTRODUCTION

Indentation methods are used to evaluate the mechanical properties of surface layers and thin films. Traditionally, a hard indenter is pressed into the specimen surface with a known force, and the hardness is estimated using the measured projected area of the resulting impression. Alternatively, in depth sensing indentations, the penetration of the indenter as a function of applied load is measured. From the resulting load versus displacement curves the material properties such as hardness and elastic modulus can be estimated.[1,2] In nanoindentation, the penetration of the indenter is of the order of nanometers. It has been found that at low penetration depths, the hardness is different from the bulk hardness and the scatter in the measurement is high.[3] Pollock *et al.*[4] have reviewed the relevant theory and the experimentation that describe the behavior of materials in the 10–1000 nm depth range.

The variation in hardness at low penetration depths may be attributed to surface chemical effects,[3,5] material property variation with depth,[3] and/or surface roughness of the specimen being indented. The variation is also influenced by the method of measurement: depth sensing or imaging and by the instrument errors in depth sensing measurement. The errors associated with nanoindentation measurement have been discussed by Menčik and Swain[6] and the scatter has been studied by Yost.[7] Here we are concerned with the effect of roughness on the surface mechanical property estimates made using nanoindentation. We would attempt in this paper to evolve a method of deconvoluting the genuine material property, from the results obtained by the nanoindentation of a rough surface.

It is not difficult to visualize as Tabor[8] had noted many years ago that the effect of roughness on hardness estimation is negligible if the indentation depths are much greater than the surface roughness. The self-affine fractal nature of engineering surfaces has been demonstrated since then using STM and AFM.[9] The roughness wavelengths that affect a physical process are determined by the length scale of the process. For nanoindentation the appropriate length scale is the size of the indent made. The effect of asperities much smaller than the indent size is averaged out, as for example in the case of conventional hardness measurements. Similarly the asperities that are much larger than the indent do not affect the measurements as they present almost a plane surface to the indenter. Polishing reduces the amplitude of roughness but at length scales greater than a certain value determined by the size of the abrasive. The power spectrum of the rough surface at high frequency (low wavelength) is unaffected by polishing. This means that except in the case of cleaved, atomistically smooth surfaces, nanoindentations are invariably and effectively carried out on rough surfaces.

For an elastic-plastic indentation, the indentation pressure depends on the imposed strain. If a cone indents a flat surface, the hardness does not change with penetration. For a spherical indenter, as the strain changes with penetration the hardness also changes with penetration. Visualizing a rough surface as made up of asperities of small radius riding on the back of asperities of larger radius,[10] penetration by indenter of any geometry brings asperities of small radius into play first (Fig. 1). With increasing penetration asperities of larger radius are encountered. As the effective radius encountered by the indenter tip continues to change with penetration, the strain varies and thus the measured hardness has to change with penetration. When nanoindentation is carried out on a rough surface, the hardness estimates are thus invariably dependent on the penetration depth. One of the key challenges here, given a description of the roughness

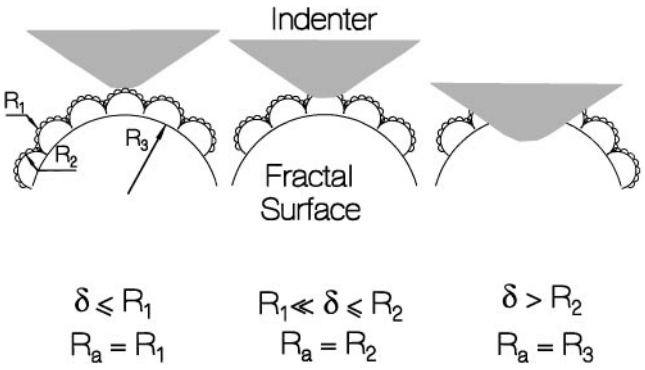

FIG. 1. Schematic of an indenter on a fractal surface. For increasing penetration depth, effective radius of curvature of the asperity increases.

and the penetration depth, is to arrive at an *ab initio* definition and therefore an estimate of the effective radius as encountered by the indenter. Such an estimate is essential for deconvoluting the surface mechanical properties from the measured nanoindentation data.

As the indenter is brought near the rough surface the contact is first established with a single asperity. When the load is increased, this asperity deforms plastically and the neighboring asperities come into contact. The contact area thus consists of many tiny islands (see Fig. 3 inset). The load versus displacement graph measured is dependent on the way in which these islands are distributed. This in turn affects the scatter in the measured property. As the load is increased, the contact islands increase both in size and number and a statistical averaging results.

In this paper we develop a roughness dependency model based on single asperity contact. The hardness estimates are experimentally validated by indenting a spherical body by a spherical indenter. The applicability of the model for a real situation is tested by comparing the roughness dependency, as suggested by the model with that obtained by numerical simulation of nanoindentation of a generated fractal surface. It is suggested that the model can be used to deconvolute the real mechanical property of a surface from experimental data by eliminating the roughness dependency.

II. INDENTATION OF A SPHERE

A. Theory

Figure 2 shows a spherical surface being indented by a spherical indenter. It has been shown[11] that the hardness estimated from such an experiment is

$$H = H_s\left(\frac{R_a \cos^2\theta}{R_i + R_a}\right), \tag{1}$$

where H_s is the hardness of the smooth flat surface and R_i and R_a are the radii of the indenter and asperity,

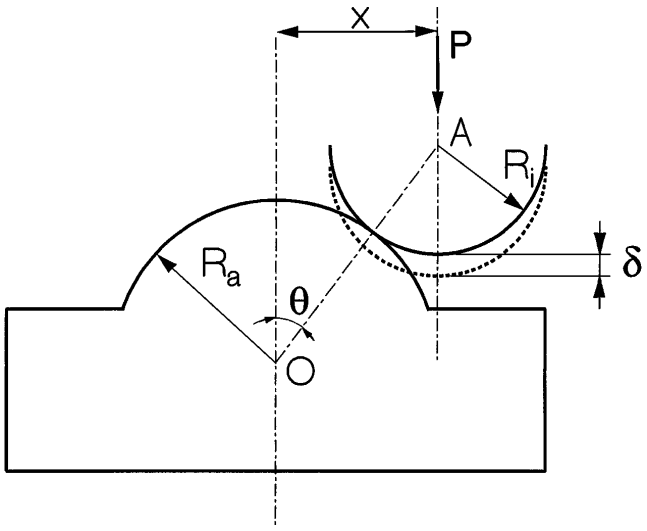

FIG. 2. Configuration of the indenter and the asperity used in the experiment. The indenter radius (R_i) = 12.5 mm. Asperity radius (R_a) = 25 mm, 12.5 mm, and 8 mm. θ was varied from 0° to 30°.

respectively. The angle θ is small, because of the presence of neighboring asperities. It further has very little effect on measured hardness. By expanding the term within the parentheses and neglecting the higher order terms of R_i/R_a (assuming $R_i \ll R_a$), the equation can be simplified to

$$\frac{H}{H_s} = 1 - \frac{R_i}{R_a}.$$

R_a varies continuously for an actual rough surface from zero to infinity as the indenter penetrates into the surface. The exact relation between R_a and the penetration depth δ depends on the nature of the rough surface. A general form of such a relation may be written as

$$R_a = K_1\left(\frac{\delta}{d_r}\right)^m, \tag{2}$$

where d_r is a roughness parameter such as root mean square roughness, with respect to which the penetration depth can be normalized. K_1 and m are the constants, dependent on the geometric nature of the rough surface. Thus,

$$\frac{H}{H_s} = 1 - \frac{K_2}{\left(\frac{\delta}{d_r}\right)^m}. \tag{3}$$

B. Experimental

Indentation experiments were carried out using a hardened steel ball of radius (R_i) 12.5 mm as the indenter. Specimens as shown in Fig. 2, and of three different radii (R_a), i.e., 25, 12.5, and 8 mm, were machined out of copper rods in a copying lathe. A fixture was used to position the specimen such that the distance between

the specimen and indenter axes (x) can be varied. Indentation was carried out in a 10 ton ($\approx$100 KN) universal testing machine, and load-displacement curves were recorded. The experimental material stiffness was found (=50 KN/m) to be two orders less than the machine stiffness of 6 GN/m. Details of the experimental setup are given in a previous paper.[12]

III. MULTIPLE ASPERITY CONTACT—NUMERICAL SIMULATION

A. Simulation

The rough surface is simulated in a way similar to that outlined by Majumdar and Tien.[13] The height variation $Z(x)$ of an isotropic and homogeneous rough surface in any arbitrary direction, along a straight line, can be represented by the Weierstrass–Mandelbrot function.[13]

$$Z(x) = G^{(D-1)} \sum_{n=n_l}^{\infty} \frac{\cos(2\pi\gamma^n x)}{\gamma^{(2-D)n}}; \qquad 1 < D < 2; \quad \gamma > 1.$$

In this G is a scaling contact, D is the fractal dimension of the profile, $\gamma^n = 1/\lambda$ is the frequency mode corresponding to the reciprocal of the wavelength (λ) of roughness, and n_l is the lower cutoff frequency of the profile which depends on the length of the sample L through the relation $\gamma^{n_l} = 1/L$; γ is chosen to be 1.5 for phase randomization and high spectral density.

This function has a power spectrum which can be approximated by a continuous spectrum[14] given by

$$P(\omega) = \frac{G^{2(D-1)}}{2\ln\gamma} \frac{1}{\omega^{(5-2D)}}.$$

The values of G and D can be obtained from a profile measurement using this expression. For isotropic surfaces, Nayak[15] has established the relation between the spectrum of a surface and its profile along an arbitrary direction. The surface spectrum[13] is

$$P^s(\omega) = \frac{(5-2D)(7-2D)}{\pi} \times \frac{G^{2(D-1)}}{2\ln\gamma} \int_0^{2\pi} \frac{\{\cos^{(5-2D)}\theta - \cos^{(7-2D)}\theta\}\, d\theta}{\omega^{(6-2D)}}.$$

The equation of the surface with this spectrum is

$$Z(x,y) = F(D)G^{(D-1)} \times \sum_{n=n_l}^{\infty} \frac{\cos(2\pi\gamma^n\{x + g(y)\})\cos(2\pi\gamma^n\{y + g(x)\})}{\gamma^{(2-D)n}}; \quad 1 < D < 2; \quad \gamma > 1, \tag{4}$$

with

$$F(D) = \left(\frac{2}{\pi} (\ln\gamma)(5-2D)(7-2D) \times \int_0^{\pi/2} \{\cos^{(5-2D)}\theta - \cos^{(7-2D)}\theta\}\, d\theta \right)^{0.5}$$

and

$$g(a) = \frac{1}{2 \times 2^{0.5}} \frac{\gamma^{(2-D)(n_l-1)}}{\{\gamma^{(4-2D)} - 1\}^{0.5}} \sum_{n=n_l}^{\infty} \frac{\cos(2\pi\gamma^n a)}{\gamma^{(2-D)n}}.$$

A value of 1.5 is chosen for D, corresponding to brownian surface.[9] The summation to infinity is cut off at a higher index. The indices are chosen to be 34 and 52, respectively, such that the roughness is simulated in the same length scale as the physical phenomena—the indentation to be studied. The surface is simulated by evaluating Eq. (4) over a grid of 128 $\times$ 128 uniformly spaced points.

The geometry of the indenter used is shown in Fig. 3. The half cone angle (ϕ) and the tip radius of curvature (R_i) are varied to get the different area functions. The surface of the indenter Z_i is generated over the same set of grid points as the simulated rough surface. The axis of the indenter is varied randomly over the x-y plane, within the 1 μm $\times$ 1 μm simulated surface.

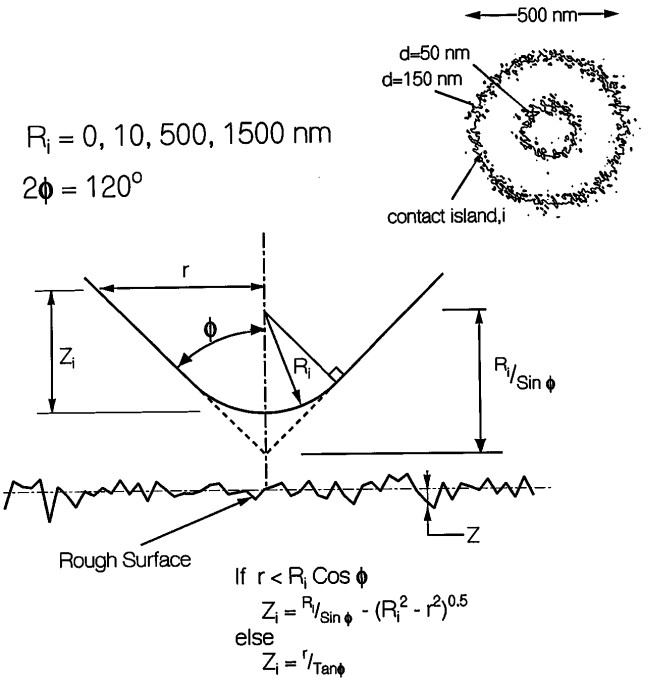

FIG. 3. Configuration of the conical indenter on a fractal surface, used in the numerical simulation. The inset shows the contact area for two penetration depths of 50 nm and 150 nm for the conical indenter with a tip radius of 10 nm.

Twenty-five such random indentations are carried out for given indenter parameters θ and R_i.

The smooth indenter is brought into contact with the simulated surface and the real contact area is obtained. For this, first the sum surface[16] is found using

$$Z_s = Z_i - Z\,.$$

Z_s gives the difference in height between the indenter Z_i and the rough surface Z (Fig. 3). The contact area for a particular penetration (δ) of the indenter into the rough surface is the contour of the sum surface for the value of Z_s equal to δ. The contours were obtained using a standard algorithm that uses linear interpolation for the Z_s values in between the grid points. A typical real contact area is shown for two penetrations in the inset of Fig. 2.

B. Contact model

The indentation of a soft, rough surface by a smooth and hard indenter is equivalent to the penetration of a soft, smooth and flat surface by a set of hard asperities.[8] From the volume and the area of a contact island, the spherical cavity model[17] is used to estimate the mean pressure acting over the contact island.

$$p_i = \frac{2}{3} Y \left\{ 2 + \left[\ln \frac{\frac{E \tan \beta}{2Y} + 2(1 - 2\nu)}{3(1 - \nu)} \right] \right\}, \quad (5)$$

where E is Young's modulus, Y is the yield strength, and ν is Poisson's ratio of the material being indented. Tanβ is obtained by equating the volume of the contact island to that of a cone of attack angle β whose base area is equal to the contact area of the island. It is assumed that the indenter deformation is negligible. The upper limit to this mean pressure is set by the condition of fully plastic deformation. Thus the load supported by each island is computed as

$$P_i = \begin{cases} p_i \times A_i & \text{if } p_i < 3 \\ 3 \times Y \times A_i & \text{if } p_i \geq 3 \end{cases}, \quad (6)$$

where A_i is the contact area of the individual islands. The total load is obtained by summing up the individual load supported by all the islands for a given penetration.

The hardness is then obtained by dividing this load with the apparent area obtained from the area function of the indenter. The penetration depth used in the area function can be obtained in two different ways, depending on the position of the reference plane. One way is to take the plane passing through the initial contact point and parallel to the mean plane of the rough surface. This simulates a depth sensing experiment with ideally infinite measurement resolution. The other way is to measure the penetration from the mean plane. This simulates the imaging type of nanoindentation experiments.[18] The area function for a given indenter geometry is computed using the same routine, but by letting the indentation be done on a smooth flat surface.

The indentation was carried out at 25 random locations on the simulated surface and the load was found out for 11 different penetration depths at a given location. The rms roughness ($R_{\rm rms}$) of the indented surface is varied by varying the magnification constant G in Eq. (4).[9] Six different rough surfaces with $R_{\rm rms}$ ranging from 0.62 nm to 2.16 nm were generated for the indentation. To introduce the effect of the varying material property with the deformation volume or the penetration depth, the yield strength Y used in Eq. (5) to calculate the mean pressure is allowed to vary as

$$Y = Y_0 \left(1 + \frac{c_0}{V^n} \right). \quad (7)$$

With $n = 1/3$ this would give, for a conical indenter, a flat surface hardness variation of type

$$H_s = H_0 \left(1 + \frac{c_1}{\delta} \right), \quad (8)$$

where H_0 is the bulk hardness and c_1 is a material constant.

IV. RESULTS AND DISCUSSION

The results of the numerical simulation of nanoindentation by a cone with a spherical tip on a fractal surface is summarized in Fig. 4. The figure clearly brings out the fact that even for a material the bulk and the surface mechanical properties of which are the same, the

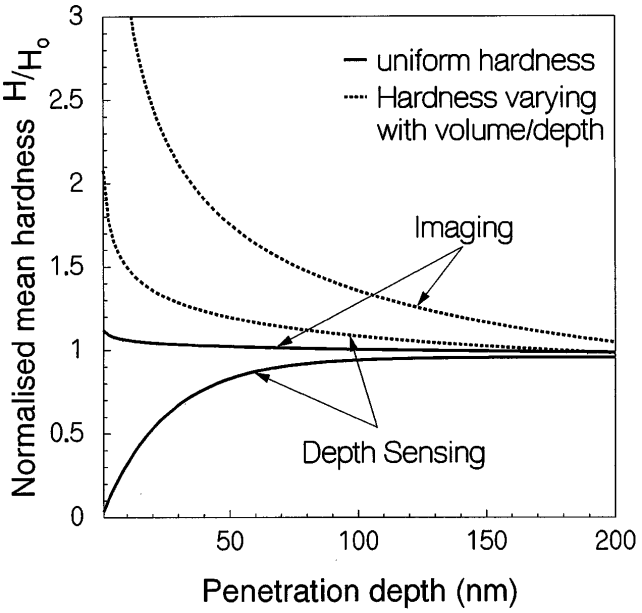

FIG. 4. Variation of mean hardness with penetration depth, obtained from numerical simulation for the conical indenter with a tip radius of 10 nm.

hardness changes with penetration as long as the surface is rough. The figure further delineates the influence of the method of measurement and the actual property gradient with depth on the measured hardness. Given this, the following explores a simple way of deconvoluting the measured data to eliminate the effect of the roughness and arrive at (for a depth sensing instrument with zero measurement error) a first order estimate of hardness characteristic with penetration which reflects genuine property variation with depth.

Figure 5 shows the experimental data collected at different angular offset (θ) and using different specimen radii (R_a) to fall roughly on a single straight line when plotted as a function of $(R_a \cos^2\theta)/(R_i + R_a)$. This validates Eq. (1). Figure 6 shows the results of indentation carried out on two spherical surfaces of the same radius but of very different heights h. The hardness of the spherical asperity whose height is equal to the radius ($h = R_a$) is independent of the penetration depth, except at very low penetration. The hardness measured by indenting the asperity whose height is equal to one-half of its radius ($h = R_a/2$), however, starts to increase as the penetration depth reaches a substantial proportion of the specimen height. The indenter beyond this stage may be visualized as encountering an effective radius which is a composite of the specimen and the flat surface radii (infinity). This simple experiment demonstrates that for a real rough surface as the indenter goes through from one level of asperity to the next layer of larger asperities, the effective radius and therefore the hardness changes.

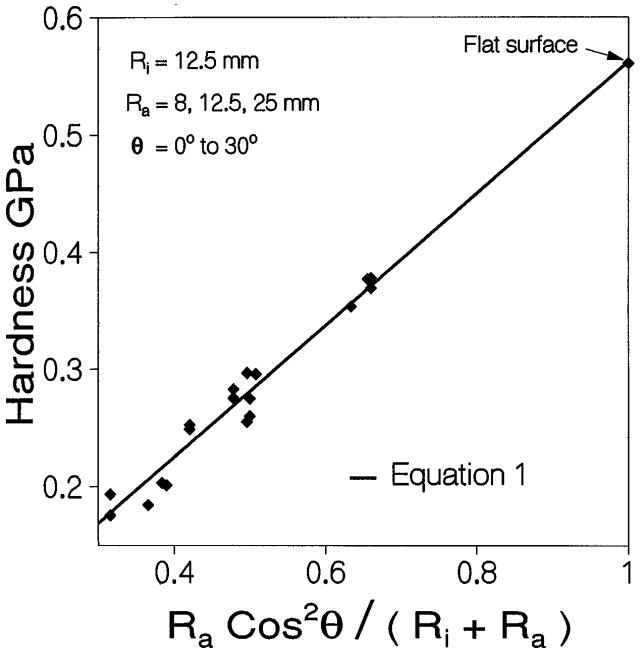

FIG. 5. Plot of hardness versus $R_a \cos^2(\theta)/(R_i + R_a)$. The experimental points lie on the line predicted by Eq. (1).

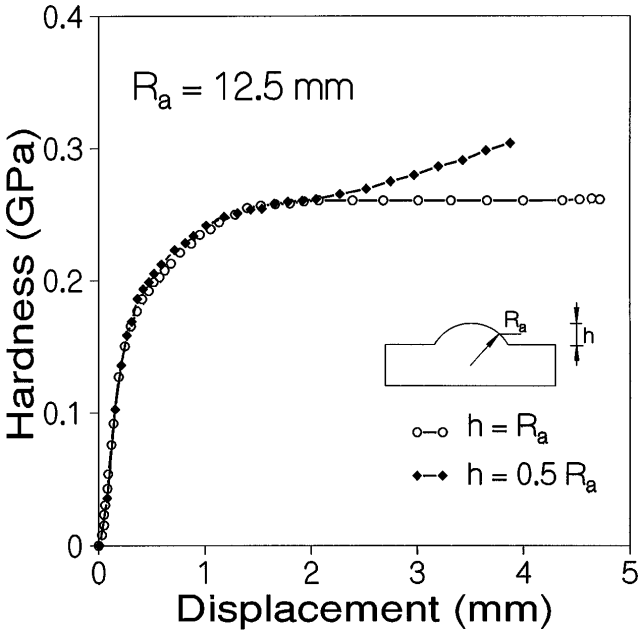

FIG. 6. Effect of varying asperity radius with penetration on measured hardness.

Weiss[19] pointed out that the effect of roughness can be accounted for, by adding an error term δ_e in displacement. This would give[11]

$$\frac{H_r}{H_0} = \frac{Af(\delta \pm \delta_e)}{Af(\delta)} = \left(1 \pm \frac{\delta_e}{\delta}\right) \quad \text{for spherical}$$

$$= \left(1 \pm \frac{\delta_e}{\delta}\right)^2 \quad \text{for conical/pyramidal},$$

where H_0 is the bulk hardness and Af is the area function of the indenter. Comparing this with Eq. (3) it is clear that for the assumed dependency of effective radius on penetration [Eq. (2)], δ_e is related to some roughness parameter and the indenter geometry. Accordingly we may write

$$\delta_e = k\,\delta_r \tag{9}$$

and

$$\frac{H_r}{H_0} = \left(1 - \frac{k}{\delta/\delta_r}\right)^n, \tag{10}$$

where k and n are parameters dependent on indenter geometry; n for Weiss's analysis is 1 for a spherical indenter and 2 for a conical indenter. The results of the numerical simulation fit Eq. (10) remarkably well for the values of k and n given in Table I. It is seen that n is an integer as predicted by Weiss,[19] and the value of k is relatively insensitive to indenter radius, both the parameters being primarily dependent on the

TABLE I. The indenter related parameters k and n obtained from numerical simulation.

	$H_r/H_0 = \left(1 - \frac{k}{(\delta/\delta_r)}\right)^n$				
	Ref: Contact point		Ref: Mean plane		
Indenter tip radius R_i nm	k	n	k	n	Remarks
1500	25.15	1	−2.21	1	Spherical
500	23.78	1	−2.28	1	Almost spherical
10	14.07	2	−4.92	2	Almost conical
0	13.29	2	−5.66	2	Conical

indenter shape. It may be noted here that k and n are not model (of the rough surface) specific and it is possible, given any measured real surface profile with proper resolution, to estimate the values of k and n by numerical simulation.

Nanoindentation of rough surfaces belonging to a material of the type given by Eq. (7) was simulated for a range of roughness (rms values). Figure 7 shows the estimated hardness points normalized with the rough surface hardness [Eq. (10)] as a function of the penetration depth and roughness, for a sharp conical indenter. The continuous lines in the figure are drawn as per the equation,

$$\frac{H_v}{H_r} = 1 + \frac{c_1}{\delta} + \frac{c_1 k \delta_r}{\delta^2}. \quad (11)$$

It is seen that the variation of hardness due to the changing roughness and penetration depth is described well by this equation. (See Appendix for a physical basis behind this equation.) Using Eq. (10) the hardness measured on a rough surface with a material property variation can be written as

$$H_v = \left(1 - \frac{k}{\delta/\delta_r}\right)^n \left(1 + \frac{c_1}{\delta} + \frac{c_1 k \delta_r}{\delta^2}\right) H_0. \quad (12)$$

The first term in this equation gives the hardness variation due to roughness alone when there is no property variation with volume/depth. The second term expresses the effect of property gradient in its interaction with roughness on hardness. This term comes about because the deformation volume in an asperity, for a given penetration depth, changes with roughness. This results in a change in the aggregate strength of the asperity. The roughness thus alters the asperity-wise distribution of strength and geometric constraint. Hardness, which is a product of strength and constraint summed over the whole contact domain, changes with roughness. When there is no property variation with volume, c_1 is zero and the hardness reduces to Eq. (10). When the roughness, on the other hand, is zero ($\delta_r = 0$) Eq. (12) reduces to the smooth surface material property profile [Eq. (8)]. Given the measured hardness, the indenter geometry related constants k_1 and n and the bulk hardness Eq. (12) can be used to determine the material constant c_1 which gives the gradient of property with depth. Although the present simulation has been done for a particular type of property profile [Eq. (8)], it is suggested that a more general profile may be determined using the approach developed here.

The scatter in the hardness measurement arising due to the roughness of the surface is found to be independent on the material property variation, but depends on the method of measurement (Fig. 8). The magnitude of the scatter can be quantified by a nondimensional parameter $S = \sigma/M$ where σ is the standard deviation and M is the mean of the values of hardness for a given penetration depth. The scatter obtained from the simulations of the imaging type of experiments is found to be less than that obtained from the simulations of the depth sensing experiment.

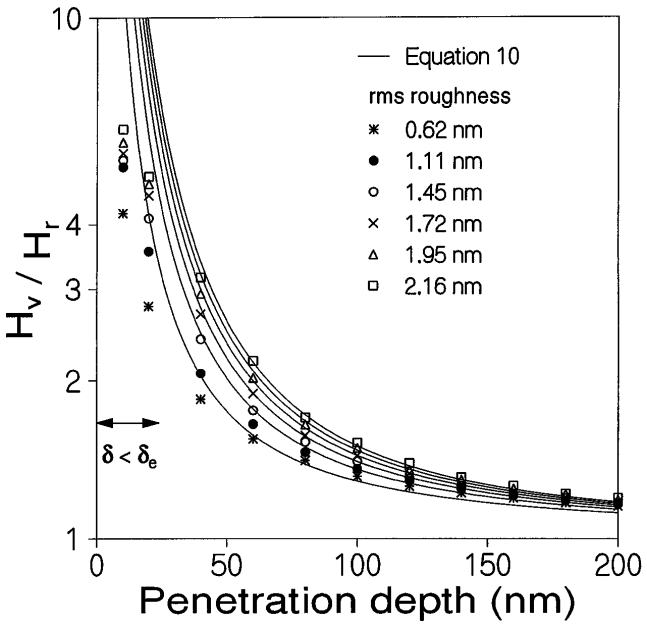

FIG. 7. Variation of mean hardness, normalized with the hardness measured on the rough surface with no property variation, with penetration depth, for the indenter with zero tip radius.

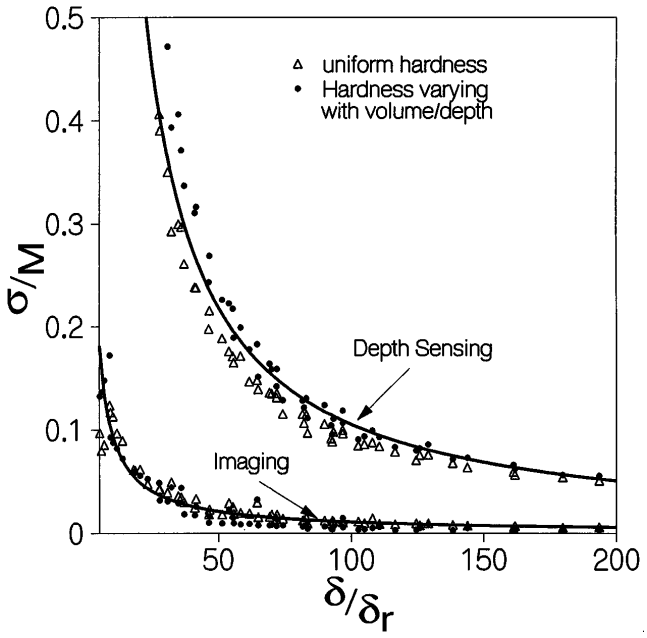

FIG. 8. Variation of the standard deviation of the measured hardness values normalized with the respective mean values, with the penetration depth normalized with rms roughness, for the indenter with 10 nm tip radius.

V. CONCLUSIONS

(1) The roughness of a surface affects the hardness estimated by nanoindentation, irrespective of whether the bulk and surface mechanical properties are the same.

(2) The effective radius of the indented fractal surface increases in direct proportion to penetration and in inverse proportion to a roughness parameter.

(3) Knowing the indenter geometry and given the roughness and penetration depth, it is possible to deconvolute the effect of roughness on measured hardness using a simple algebraic equation, to determine the genuine mechanical property profile of the surface region.

REFERENCES

1. M. F. Doerner and W. D. Nix, J. Mater. Res. **1**, 601 (1986).
2. J. L. Loubet, J. M. Georges, and G. Meille, in *Microindentation Techniques in Materials Science and Engineering,* ASTM STP 889, edited by P. J. Blau and B. R. Lawn (American Society for Testing and Materials, Philadelphia, PA, 1986), p. 72.
3. W. C. Oliver, R. Hutchings, and J. B. Pethica, in *Microindentation Techniques in Materials Science and Engineering,* ASTM STP 889, edited by P. J. Blau and B. R. Lawn (American Society for Testing and Materials, Philadelphia, PA, 1986), p. 90.
4. H. M. Pollock, D. Maugis, and M. Barquins, in *Microindentation Techniques in Materials Science and Engineering,* ASTM STP 889, edited by P. J. Blau and B. R. Lawn (American Society for Testing and Materials, Philadelphia, PA, 1986), p. 47.
5. W. W. Gerberich, S. K. Venkataramanan, H. Huang, S. E. Harrey, and D. L. Kohlstedt, Acta Metall. Mater. **43**, 1569 (1995).
6. J. Menčik and M. V. Swain, J. Mater. Res. **10**, 1491 (1995).
7. F. G. Yost, Metall. Trans. **14A**, 947 (1983).
8. D. Tabor, *The Hardness of Metals* (Oxford University Press, Glasgow, 1951).
9. A. Mujamdar and B. Bhusan, Trans. ASME, J. Tribology **112**, 205 (1990).
10. J. F. Archard, Proc. Roy. Soc. London **A243**, 190 (1957).
11. M. S. Bobji, M. Fahim, and S. K. Biswas, Trib. Lett. **2**, 381 (1996).
12. M. S. Bobji and S. K. Biswas, Philos. Mag. A **73**, 399 (1996).
13. A. Majumdar and C. L. Tien, Wear **136**, 313 (1990).
14. M. V. Berry and Z. V. Lewis, Proc. Roy. Soc. London **A370**, 459 (1980).
15. P. R. Nayak, Wear **26**, 165 (1973).
16. H. A. Fransis, Wear **45**, 221 (1977).
17. K. L. Johnson, *Contact Mechanics* (Cambridge University Press, Cambridge, 1985).
18. B. Bhusan, V. N. Koinkar, and J-A. Ruan, Proc. Instn. Mech. Engrs. **J1**, **208**, 17 (1994).
19. H. J. Weiss, Phys. Status Solidus **A129**, 167 (1992).

APPENDIX

For a rough surface with a material property variation of type given by Eq. (7), the effect of roughness can be introduced by adding an error term δ_e to the penetration depth. Thus, from Eq. (8), for a sharp conical indenter,

$$H_v = H_r\left(1 + \frac{c_1}{\delta - \delta_e}\right).$$

Substituting for δ_e from Eq. (9), this can be written in a series form for $\delta > \delta_e$ as

$$H_v = H_r\left(1 + \frac{c_1}{\delta} + \frac{c_1 k\,\delta_r}{\delta^2} + \frac{c_1(k\,\delta_r)^2}{\delta^3} + \cdots\right).$$

Equation (12) is obtained from the above equation by neglecting higher order terms and by substituting for H_r from Eq. (10).